Heat rectification in molecular junctions

Dvira Segal[a] and Abraham Nitzan
School of Chemistry, Tel Aviv University, Tel Aviv, 69978, Israel

(Received 25 January 2005; accepted 9 March 2005; published online 16 May 2005)

Heat conduction through molecular chains connecting two reservoirs at different temperatures can be asymmetric for forward and reversed temperature biases. Based on analytically solvable models and on numerical simulations we show that molecules rectify heat when two conditions are satisfied simultaneously: the interactions governing the heat conduction are nonlinear, and the junction has some structural asymmetry. We consider several simplified models where a two-level system (TLS) simulates a highly anharmonic vibrational mode, and asymmetry is introduced either through different coupling of the molecule to the contacts, or by considering internal molecular asymmetry. In the first case, we present *analytical* results for the asymmetric heat current flowing through a *single* anharmonic mode using different forms for the TLS-reservoirs coupling. We also demonstrate numerically, studying a realistic molecular model, that a uniform anharmonic molecular chain connecting asymmetrically two thermal reservoirs rectifies heat. This effect is stronger for longer chains, where nonlinear interactions dominate the transfer process. When asymmetry is related to the internal level structure of the molecule, numerical simulations reveal a nontrivial rectification behavior. We could still explain this behavior in terms of an effective system-bath coupling. Our study suggests that heat rectification is a fundamental characteristic of asymmetric nonlinear thermal conductors. This phenomenon is important for heat control in nanodevices and for understanding of energy flow in biomolecules. © *2005 American Institute of Physics*. [DOI: 10.1063/1.1900063]

I. INTRODUCTION

Rectifiers, devices that transport current efficiently in one direction of the applied bias, while blocking it completely or significantly in the reverse direction, have been commonly associated with electron transfer. *Molecular electronics* rectifiers, first proposed by Aviram and Ratner,[1] have been studied and demonstrated in different metal-molecule metal structures.[2–5] While different rectification mechanisms have been identified and discussed, the common feature characterizing such molecular electronics devices is an underlying structural asymmetry that leads to different potential profiles along the junction for the opposite bias directions.

Motivated by the growing interest in nanomechanics—construction and study of nanolevel mechanical devices—we investigate theoretically the analogous concept of a molecular level *heat* rectifier, a molecular device that conducts energy current asymmetrically upon reversing the temperature bias. We discuss the origin of such heat transport asymmetry, essentially asymmetric phonon transfer for forward and reverse temperature bias, its dependence on junction characteristics, and its relationship to the way the temperature is distributed along the junction under steady-state operation. Other mechanical devices that have been discussed recently are heat engines,[6–8] motors,[9,10] and even a mechanical analog of a laser.[11] Experimentally, nanostructures have become accessible for heat transfer measurements,[12,13] enabling study of the thermal conductivity of single molecules, e.g., a carbon nanotube.[14]

From the theoretical perspective, different aspects of heat transport in nanojunctions including single molecule devices were investigated in recent years. Some of these studies that are relevant to the present discussion are reviewed below.

Historically, intramolecular vibrational redistribution (IVR) phenomena in vibrationally excited molecules have been subjects of intensive studies in the past two decades. The main objective of these investigations is to expose the important vibrational pathways to chemical reactions and the possibility to control such processes.[15] The key issues in these studies involve the transfer of vibrational energy between different molecular modes and the relaxation of local mode excitations to the rest of the molecular vibrational subspace. Of particular interest are the recent investigations by Schwarzer *et al.*[16,17] of IVR in bridged azulene-anthracene structures. This work constitutes an important link between IVR measurements and the traditional concepts of heat transport theory: the coefficient of thermal conductivity and diffusive versus ballistic modes of energy transfer.

From a different perspective, there has been a long-time effort aimed at understanding the relationship between phonon transport in constrained nanosystems, specifically one-dimensional (1D) conductors, and the phenomenological Fourier law of heat conduction, $J=-K\nabla T$, that connects the heat flux J to the local temperature gradient ∇T through the thermal conductance K. The ultimate goal of these investigations is to derive this macroscopic law from statistical-mechanics arguments, and find how it applies in the low-dimensional regime. Following Rieder, Lebowitz, and Lieb[18] and Zürcher and Talkner[19] who found that heat flux in harmonic systems is proportional to the temperature difference

[a]Author to whom correspondence should be addressed. Present address: Department of Chemical Physics, the Weizmann Institute of Science, Rehovot 76100, Israel. Electronic mail: dvira.segal@weizmann.ac.il

rather than the temperature gradient (implying that thermal conductivity diverges with increasing chain length), there were many studies of "anomalous heat conduction" in 1D systems and models for recovery of the Fourier law were investigated.[20–25] For a recent review see Ref. 26.

Quantum aspects of heat conductance were theoretically investigated and experimentally manifested in recent years. The existence of a universal quantum of thermal conductance, $g=\pi^2k_B^2T/3h$, has been predicted[27] and experimentally confirmed.[28] Here k_B and h are the Boltzmann and Planck constants, respectively, and T is the temperature. For ballistic phonon transfer, a two-terminal Landauer-type formula for thermal flux has been derived,[27,29,30] and later generalized to the four-terminal case.[31] This relationship, an analog of the Landauer formula for electrical conduction in nanojunctions,[32] describes energy transfer between two [left (L), right (R)] thermal reservoirs maintained at equilibrium with the temperatures T_L and T_R, respectively, in terms of the temperature-independent transmission coefficient $\mathcal{T}(\omega)$ for phonons of frequency ω,

$$J=\int \mathcal{T}(\omega)[n_L(\omega)-n_R(\omega)]\omega d\omega. \tag{1}$$

Here $n_K(\omega)=(e^{\beta_K\omega}-1)^{-1}$; $\beta_K=(k_BT_K)^{-1}$; $K=L,R$ $(\hbar\equiv 1)$ are the Bose Einstein distribution functions characterizing the reservoirs.

Because $\mathcal{T}(\omega)$ is temperature independent for ballistic transport, Eq. (1) is symmetric to interchanging the reservoirs temperatures. Consequently, systems obeying this expression, for example, harmonic chains, cannot show rectifying behavior irrespective of any structural asymmetry. A natural question is then what are the minimal conditions needed in order to manifest heat rectification. Similar concerns were raised for molecular level electrical rectifiers, where it was established that in order to exhibit diodelike behavior the junction has to combine geometric asymmetry with a characteristic voltage drop distribution across the molecular bridge.[33,34] It is important to note that this dependence on the electrostatic potential distribution that itself depends on the bias direction is a manifestation of electron-electron interaction, i.e., of nonlinear interactions in the junction.

In this work we focus on heat transfer in nanojunctions and show that similarly to the electrical case, two conditions are required for *heat* rectification: first, the conducting chain needs to have some built-in asymmetry and, secondly, nonlinear interactions should govern the energy transfer. When these conditions are both satisfied, they may result in an internal temperature drop across the molecule with different temperature profiles for forward and reversed temperature biases. Terraneo *et al.*[35] had demonstrated these effects on a lattice made of a highly nonlinear region sandwiched between two anharmonic and asymmetric domains using classical Langevin simulations. Recently, we have also theoretically analyzed similar effects on a simplified two-level system simulating a single highly anharmonic vibrational mode.[36] There, in analogy to Ref. 37, the system asymmetry was introduced by imposing different coupling strengths to the L and R thermal reservoirs.

In this paper we first give a detailed account of the simplified model discussed in Ref. 36. We then extend the model to study heat rectification on a molecular junction with an internal structure. We show that heat rectification can occur in junctions characterized by inherent structural asymmetry, as opposed to earlier studies where the asymmetry stemmed from different couplings to the heat reservoirs. In all cases, nonlinearity, such as associated with anharmonic interactions, is required as discussed above. We note in passing that directionally biased heat conduction will be potentially useful in electrical nanodevices where efficient heat transfer away from the conductor center is crucial for proper functionality and stability. Similarly, directed energy flow in biomolecules, such as proteins,[38] may play a role in controlling conformational dynamics.

The paper is organized as follows: in Sec. II we study the rectification emerging from system-reservoir asymmetric coupling. We analyze the simplest nonlinear conductor: a two-level system (TLS), for which the heat conduction behavior can be resolved using analytic approximations. We also exemplify rectification on a realistic molecular chain using Langevin dynamics simulations. In Sec. III we show that a molecule with an asymmetric internal level structure can operate as an asymmetric heat conductor molecule made of unequal two separate segments. Section IV concludes.

II. RECTIFICATION: ASYMMETRIC SYSTEM-BATH COUPLING

Here we present analytical and numerical results that indicate that an anharmonic molecular system coupled asymmetrically to two thermal baths can operate as a heat rectifier. We study two anharmonic models. The first is essentially a generalization of the spin-boson model[39] in which a two-level system is coupled to two equilibrium boson baths maintained at different temperatures. Such a two-level system may be a truncated version of a general anharmonic system, e.g., an anharmonic vibration or a local molecular libration, where at low temperature only the lowest quantum states are relevant. We study two variants of the model and show that if asymmetry is built into either one by employing different spin-boson coupling strengths for the two baths, thermal rectification naturally sets in. We also study heat transfer through a chain of N identical anharmonic oscillators connecting asymmetrically two heat baths by using the classical Langevin dynamics. Also in this case, with no spectral truncation involved, we find rectifying transport behavior. This shows that thermal rectification is a general characteristic of anharmonic asymmetric molecular junctions.

A. Spin-boson model I

A TLS may be considered as a model of the highest anharmonicity. We describe its interaction with two thermal baths using a spin-boson Hamiltonian,

$$H=E_0|0\rangle\langle 0|+E_1|1\rangle\langle 1|+H_B+H_{MB}, \tag{2}$$

$$H_B=H_L+H_R;\ H_K=\sum_{j\epsilon K}\omega_j a_j^\dagger a_j;\ K=L,R, \tag{3}$$

$$H_{MB} = B|0\rangle\langle 1| + B^{\dagger}|1\rangle\langle 0|;\ B = B_L + B_R, \tag{4}$$

where $a_j^{\dagger}$, a_j are the boson creation and annihilation operators associated with the phonon modes of the two harmonic baths and B_K are the bath operators, e.g., for a linear coupling model,

$$B_K = B_K^{\dagger} = \sum_{j\epsilon K} \overline{a}_j x_j, \quad x_j = (2\omega_j)^{-1/2}(a_j^{\dagger} + a_j), \quad K = L,R. \tag{5}$$

Asymmetry is incorporated by taking $\overline{\alpha}_{j\epsilon L} \neq \overline{\alpha}_{j\epsilon R}$. An important attribute of this model, shared by most studied transport models of this kind, is that the transport processes at the two system-bath interfaces are independent of each other and can be handled separately to a very good approximation.

It is convenient to regard the model (2)–(5) as a special case of an N equally spaced states system with nearest-neighbor coupling through the two heat baths $H_{MB} = \Sigma_{n=1}^{N-1}\sqrt{n}(B|n-1\rangle\langle n| + B^{\dagger}|n\rangle\langle n-1|)$. In particular the $N\to\infty$ limit with equal-energy spacing corresponds to a harmonic-oscillator bridge connecting the baths. Equation (5) corresponds in the latter case to the bilinear coupling model with the oscillator-bath interactions given by $H_{MB} = \Sigma_{j\epsilon K} a_j x_j x$ ($K = L,R$). x is the coordinate of the bridge oscillator and $\alpha_j = \overline{\alpha_j}(2m\omega_0)^{1/2}$ where m and $\omega_0 = E_1 - E_0$ are the oscillator mass and frequency, respectively.

The reduced dynamics in the space of the N-level system can be derived following standard procedures, e.g., the Redfield approximation[40] for the weak system-bath coupling limit. The resulting kinetic equations for the state probabilities, in the Markovian limit and assuming that coherences can be disregarded on the relevant time scale, can be written in the unified form,

$$\dot{P}_n = -[nk_d + (n+1)k_u X_n]P_n + nk_u P_{n-1} + (n+1)k_d X_n P_{n+1}, \tag{6}$$

where $X_n = \delta_{n,0}$ for the two-level ($n = 0,1$) system and $X_n = 1$ for the harmonic-oscillator ($n = 0,\ldots,\infty$) case. The rate constants for vibrational excitation and relaxation are given by

$$k_u = \int_{-\infty}^{\infty} d\tau e^{-i\omega_0\tau}\langle B(\tau)B^{\dagger}(0)\rangle,$$

$$k_d = \int_{-\infty}^{\infty} d\tau e^{-i\omega_0\tau}\langle B^{\dagger}(\tau)B(0)\rangle. \tag{7}$$

The average is done over the thermal distributions of the baths. Equation (6) is obtained irrespective of the fact that the average in (7) may involve several baths kept at different temperatures.[41] Specifying to the case of two baths with temperatures $T_L = 1/k_B\beta_L$ and $T_R = 1/k_B\beta_R$ and to linear coupling, and assuming that there is no correlation between the two thermal baths leads to

$$\dot{P}_n = -[nk_L + nk_R + (n+1)(k_L e^{-\beta_L\omega_0} + k_R e^{-\beta_R\omega_0})X_n]P_n + (n+1)(k_L + k_R)X_n P_{n+1} + n(k_L e^{-\beta_L\omega_0} + k_R e^{-\beta_R\omega_0})P_{n-1} \tag{8}$$

with

$$k_L = \Gamma_L(\omega_0)[1 + n_L(\omega_0)], \quad k_R = \Gamma_R(\omega_0)[1 + n_R(\omega_0)], \tag{9}$$

where Γ_L and Γ_R are the temperature-independent rates given by

$$\Gamma_K(\omega) = \frac{\pi}{2m\omega^2}\sum_{j\in K}\alpha_j^2\delta(\omega - \omega_j), \quad K = L,R. \tag{10}$$

In what follows we assume that heat transfer is dominated by resonance energy transmission and that dephasing processes are fast enough so that the dynamics is fully described by the master equation (8). The heat conduction properties in this limit are then obtained from the steady-state solution of this equation.

Consider first the harmonic model ($N\to\infty$). A steady-state solution of Eq. (8) is obtained by putting $\dot{P}_n = 0$ for all n. On searching a solution of the form $P_n \propto y^n$ we get a quadratic equation for y whose physically acceptable solution is

$$y = \frac{k_L e^{-\beta_L\omega_0} + k_R e^{-\beta_R\omega_0}}{k_L + k_R}. \tag{11}$$

This leads to the normalized state populations,

$$P_n = (1-y)y^n, \tag{12}$$

and to the average steady-state population [using the linear coupling form, Eq. (9)],

$$P_T = \sum_{n=0}^{\infty} nP_n = \frac{\Gamma_L n_L + \Gamma_R n_R}{\Gamma_R + \Gamma_L}, \tag{13}$$

where the thermal distributions and the rate coefficients are evaluated at the frequency ω_0. The steady-state heat flux is obtained from

$$J = -\omega_0\sum_{n=1}^{\infty} n(k_L P_n - k_L P_{n-1}e^{-\beta_L\omega_0}) = \omega_0\sum_{n=1}^{\infty} n(k_R P_n - k_R P_{n-1}e^{-\beta_R\omega_0}), \tag{14}$$

where the positive sign indicates current going from left to right. Using Eqs. (9), (11), and (12) we find

$$J = \omega_0\frac{\Gamma_L\Gamma_R}{\Gamma_R + \Gamma_L}(n_L - n_R). \tag{15}$$

This is a special case of Eq. (1) [with $\mathcal{T}(\omega) = \Gamma_L\Gamma_R(\Gamma_L + \Gamma_R)^{-1}\delta(\omega - \omega_0)$, consistent with our resonance energy-transfer assumption], which obviously cannot exhibit any rectifying behavior.[42] Analogous results are obtained for electron transmission through double barrier resonance tunneling devices,[43,44] where in the wideband regime the electric current is proportional to $\Gamma_L\Gamma_R/(\Gamma_R + \Gamma_L)$, $\Gamma_{L/R}$ is the elastic coupling to the leads, irrespective of inelastic effects.

Next consider the two-level case, $N = 2$. The two steady-state equations obtained from Eq. (8) yield

$$P_1 = \frac{k_L e^{-\beta_L\omega_0} + k_R e^{-\beta_R\omega_0}}{k_L(1 + e^{-\beta_L\omega_0}) + k_R(1 + e^{-\beta_R\omega_0})}, \quad P_1 = 1 - P_0, \tag{16}$$

and the analog of Eq. (14) is

$$J = -\omega_0(k_L P_1 - k_L P_0 e^{-\beta_L \omega_0}) = \omega_0(k_R P_1 - k_R P_0 e^{-\beta_R \omega_0}). \tag{17}$$

This leads to

$$J = \omega_0 \frac{k_L k_R (e^{-\beta_L \omega_0} - e^{-\beta_R \omega_0})}{k_L(1 + e^{-\beta_L \omega_0}) + k_R(1 + e^{-\beta_R \omega_0})} \tag{18}$$

and, using Eq. (9), results in

$$J = \omega_0 \frac{\Gamma_L \Gamma_R (n_L - n_R)}{\Gamma_L(1 + 2n_L) + \Gamma_R(1 + 2n_R)}. \tag{19}$$

Equation (19) is an expression for the energy current through our two-level system. In contrast with the harmonic-oscillator result (15), Eq. (19) is not antisymmetric under the exchange of T_L and T_R if $\Gamma_L \neq \Gamma_R$. Indeed, defining the asymmetry parameter χ such that

$$\Gamma_L = \Gamma(1 - \chi), \quad \Gamma_R = \Gamma(1 + \chi), \quad -1 \leqslant \chi \leqslant 1, \tag{20}$$

we find

$$\Delta J \equiv J(T_L = T_h; T_R = T_c) + J(T_L = T_c; T_R = T_h) = \frac{\omega_0 \Gamma \chi (1 - \chi^2)(n_h - n_c)^2}{(1 + n_h + n_c)^2 - \chi^2 (n_h - n_c)^2}, \tag{21}$$

where T_c and T_h are the temperatures of the cold and hot reservoirs and n_c and n_h are the Bose–Einstein thermal distributions calculated at the respective temperatures. This result shows several interesting features:

(a) In the deep quantum limit, T_h, $T_c \ll \omega_0/k_B$, rectification decreases exponentially with the frequency and the inverse temperatures, $\Delta J \sim \omega_0 (e^{-\omega_0/k_B T_h} - e^{-\omega_0/k_B T_c})^2$.

(b) In the opposite, highly classical limit, T_c, $T_h \gg \omega_0/k_B$, Eq. (21) yields $\Delta J \sim \omega_0 \Delta T^2/(T_c + T_h)^2$, with $\Delta T = T_h - T_c$, implying that asymmetry increases linearly with $(\Delta T)^2$ and ω_0. The same dependence on $(\Delta T)^2$ is obtained in the $\Delta T \to 0$ limit.

(c) In the intermediate regime, T_c, $T_h \sim \omega_0/k_B$, rectification *decreases* with ω_0, $\Delta J \sim \Delta T^2/\omega_0$.

(d) Noting that $\mathrm{sign}(\Delta J) = \mathrm{sign}(\chi)$ it follows from Eq. (20) that the current is larger when the bridge links more strongly to the colder reservoir than when it links more strongly to the hotter one. This behavior can be understood by defining an effective, temperature-dependent coupling constant $\tilde{\Gamma}_K = \Gamma_K(1 + 2n_K)$; $K = L, R$. Then the heat current from Eq. (19) can be recast in the form similar to the harmonic expression (15),

$$J = \omega_0 \frac{\tilde{\Gamma}_L \tilde{\Gamma}_R}{\tilde{\Gamma}_L + \tilde{\Gamma}_R} \left[\frac{n_L - n_R}{(1 + 2n_L)(1 + 2n_R)} \right]. \tag{22}$$

For $\Gamma_L \gg \Gamma_R$ and $T_L > T_R$, for example, the energy current is proportional to the effective coupling at the right side, or $J \propto T_c$ in the classical limit. When reversing the temperature bias we get $J \propto T_h$. Thus the ratio between the oppositely going currents is $\sim T_c/T_h$.

Figure 1 depicts an example of this behavior. Shown is the ratio $\Delta J/J_0$ (with $J_0 = |J(\chi = 0)|$) plotted against the temperature T_c, while keeping T_h fixed. In Fig. 2 we show the rectification ratio against the asymmetry parameter χ for different TLS frequencies. Note that the value of Γ is not important when we consider rectification ratio, and that the heat current for the symmetric $\Gamma_L = \Gamma_R$ system is at the 10^{14} cm^{-1}/s range.

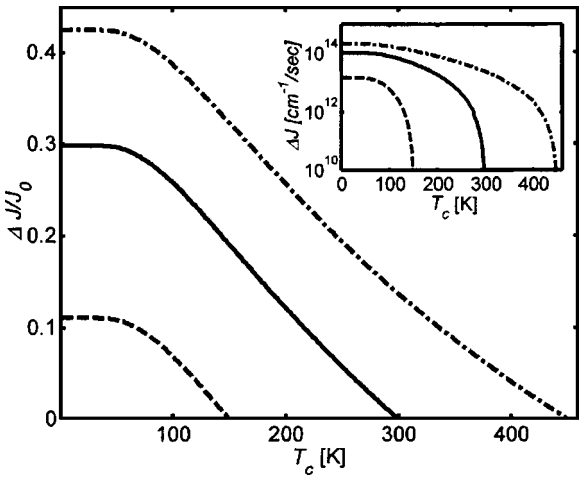

FIG. 1. Heat rectification by a TLS bridge in the linear coupling model, described by Eqs. (2)–(21). The ratio $\Delta J/J_0$ is plotted against T_c while the hot reservoir is kept at a fixed temperature: $T_h = 150$ K (dashed), $T_h = 300$ K (full) and $T_h = 450$ K (dash-dotted), $\omega_0 = 200$ cm^{-1}, and $\chi = 1/2$. The inset shows ΔJ for the three cases.

B. Spin-boson model II

Next we consider another variant of the two-bath spin-boson model, taking the Hamiltonian to be

$$H = E_0|0\rangle\langle 0| + E_1|1\rangle\langle 1| + V_{0,1}|0\rangle\langle 1| + V_{1,0}|1\rangle\langle 0| + \sum_{j \epsilon L,R} \omega_j a_j^\dagger a_j + \sum_{j \epsilon L,R} x_j(\alpha_{0,j}|0\rangle\langle 0| + \alpha_{1,j}|1\rangle\langle 1|). \tag{23}$$

The two boson baths, L and R, are maintained at different temperatures T_L and T_R. Note that if $T_L = T_R$, i.e., when the TLS is coupled to a single thermal bath, Eq. (23) represents a standard spin-boson Hamiltonian used, e.g, in the electron transfer problem. Using the small polaron transformation,[45]

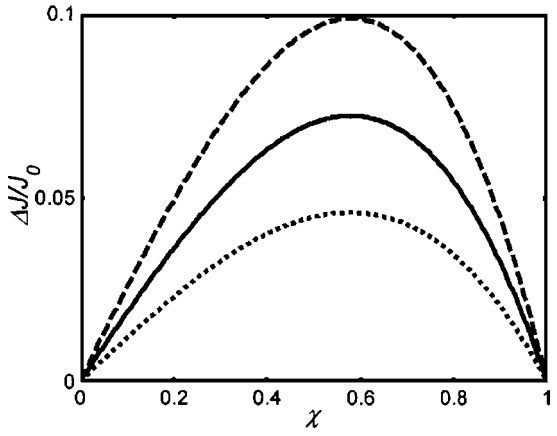

FIG. 2. The ratio $\Delta J/J_0$ vs the asymmetry parameter χ for several two-level bridges characterized by different level spacing ω_0: dashed line $\omega_0 = 200$ cm^{-1}; full line $\omega_0 = 400$ cm^{-1}; dotted line $\omega_0 = 600$ cm^{-1}. The bath temperatures are $T_h = 400$ K and $T_c = 300$ K.

$$\tilde{H} = UHU^{-1}, \quad U = U_0 U_1, \tag{24}$$

where, for $n=0, 1$,

$$U_n = \exp(-i|n\rangle\langle n|\Omega_n), \quad \Omega_n = \Omega_n^L + \Omega_n^R, \tag{25}$$

$$\Omega_n^K = i\sum_{j\in K} \lambda_{n,j}(a_j^\dagger - a_j) \ (K = L,R), \quad \lambda_{n,j} = (2\omega_j^3)^{-1/2}\alpha_{n,j} \tag{26}$$

leads to

$$\tilde{H} = E_0|0\rangle\langle 0| + E_1|1\rangle\langle 1| + V_{0,1}|0\rangle\langle 1|e^{i\Omega} + V_{1,0}|1\rangle\langle 0|e^{-i\Omega} + \sum_{j\epsilon L,R} \omega_j a_j^\dagger a_j + H_{\text{shift}}, \tag{27}$$

where $\Omega = \Omega_1 - \Omega_0$ and $H_{\text{shift}} = -(1/2)\Sigma_j \omega_j^{-2}(\alpha_{0,j}^2|0\rangle\langle 0| + \alpha_{1,j}^2|1\rangle\langle 1|)$ may be henceforth incorporated into the zero-order energies.

The Hamiltonian (27) is similar to that defined in Eqs. (2)–(4), however, here the system-bath couplings appear as multiplicative factors rather than as additive contributions in the interaction term, therefore the transport processes associated with these couplings are nonseparable. The dynamics may still be readily handled. For small V (the "nonadiabatic limit") the Hamiltonian (27) implies again rate equation (6) with the rates k_d and k_u given by

$$k_d = |V_{0,1}|^2 C(\omega_0), \quad k_u = |V_{0,1}|^2 C(-\omega_0), \tag{28}$$

where $\omega_0 = E_1 - E_0$ and $C(\omega_0) = \int_{-\infty}^{\infty} dt e^{i\omega_0 t}\tilde{C}(t)$ with

$$\begin{aligned}\tilde{C}(t) &= \langle e^{i\Omega(t)}e^{-i\Omega(0)}\rangle \\ &= \langle e^{i[\Omega_1^L(t)-\Omega_0^L(t)]}e^{-i[\Omega_1^L(0)-\Omega_0^L(0)]}\rangle_L \\ &\quad \times \langle e^{i[\Omega_1^R(t)-\Omega_0^R(t)]}e^{-i[\Omega_1^R(0)-\Omega_0^R(0)]}\rangle_R.\end{aligned} \tag{29}$$

This may be evaluated explicitly to give

$$\tilde{C}(t) = \tilde{C}_L(t)\tilde{C}_R(t), \quad \tilde{C}_K(t) = \exp[-\phi_K(t)], \quad K = L,R, \tag{30}$$

$$\phi_K(t) = \sum_{j\epsilon K} (\lambda_{1,j} - \lambda_{0,j})^2\{[1 + 2n_K(\omega_j)] - [1 + n_K(\omega_j)]e^{-i\omega_j t} - n_K(\omega_j)e^{i\omega_j t}\}, \quad K = L,R. \tag{31}$$

Explicit expressions may be obtained using the short-time approximation (valid for $\Sigma_{j\epsilon K}(\lambda_{1,j}-\lambda_{0,j})^2 \gg 1$ and/or at high temperature) whereupon $\phi(t)$ is expanded in powers of t keeping terms up to order t^2. This leads to

$$C(\omega_0) = \sqrt{\frac{2\pi}{(D_L^2 + D_R^2)}}\exp\left[-\frac{(\omega_0 - E_M^L - E_M^R)^2}{2(D_L^2 + D_R^2)}\right], \tag{32}$$

where $(K = L, R)$

$$E_M^K = \sum_{j\epsilon K} (\lambda_{1,j} - \lambda_{0,j})^2\omega_j, \tag{33}$$

$$D_K^2 = \sum_{j\epsilon K} (\lambda_{1,j} - \lambda_{0,j})^2\omega_j^2[2n_K(\omega_j) + 1] \xrightarrow{\omega/k_B T_K \to 0} 2k_B T_K E_M^K. \tag{34}$$

Equations (28)–(34) provide an extension of the Marcus nonadiabatic rate expressions[46] to the case of two reservoirs maintained at different temperatures. E_M^L and E_M^R are the corresponding reorganization energies.

Next consider the steady-state heat current in this model. What makes this a unique transport problem is the nonseparability of the system-bath couplings that makes the procedure that leads to Eq. (17) unusable. Instead we note that $C_L(\omega_0)$ and $C_R(\omega_0)$ are essentially the rates affected by each thermal reservoir separately and that from Eq. (30) $C(\omega_0) = \int_{-\infty}^{\infty} d\omega C_L(\omega_0 - \omega)C_R(\omega)$. It follows that the process $|1\rangle \to |0\rangle$ in which the TLS loses energy ω_0 can be viewed as a combination of processes in which the system gives energy ω (or gains it if $\omega < 0$) to the right bath and energy $\omega_0 - \omega$ to the left one, with probability $C_L(\omega_0 - \omega)C_R(\omega)$. A similar analysis applies to the process $|0\rangle \to |1\rangle$. The heat flux calculated as the energy transferred per unit time into the right bath is therefore[47]

$$\begin{aligned}J &= |V_{0,1}|^2 \int_{-\infty}^{\infty} d\omega\omega C_R(\omega)[C_L(\omega_0 - \omega)P_1 + C_L(-\omega_0 - \omega)P_0] \\ &= |V_{0,1}|^2 \int_{-\infty}^{\infty} d\omega\omega[C_R(\omega)C_L(\omega_0 - \omega)P_1 - C_R(-\omega) \\ &\quad \times C_L(-\omega_0 + \omega)P_0],\end{aligned} \tag{35}$$

where $P_0 = C(\omega_0)/[C(\omega_0) + C(-\omega_0)]$ and $P_1 = 1 - P_0$ are the steady-state probabilities that the system is in state 0 or 1, respectively.

Equation (35) can be evaluated numerically. Further progress on the analytical level can be made by invoking the short-time approximation in which $C(\omega)$ takes the form

$$C_K(\omega) = (D_K^2)^{-1/2}\exp[-(\omega - E_M^K)^2/(2D_K^2)], \quad K = L,R. \tag{36}$$

Using this in (35) leads to

$$J = 4k_B|V_{0,1}|^2 \frac{\sqrt{2\pi}}{(D_L^2 + D_R^2)^{3/2}} \frac{e^{-(\omega_0 - E_M^L - E_M^R)^2/2(D_L^2+D_R^2)}}{1 + e^{2\omega_0(E_M^L+E_M^R)/(D_L^2+D_R^2)}} \times E_M^L E_M^R(T_L - T_R). \tag{37}$$

It is convenient also to take $E_M^L = E_M(1-\chi)$; $E_M^R = E_M(1+\chi)$ $(|\chi| \leqslant 1)$, which implies $D_L^2 + D_R^2 = 2k_B E_M(T_S - \chi\Delta T)$ where $\Delta T = T_L - T_R$; $T_S = T_L + T_R$. This leads to

$$J = \frac{2\sqrt{\pi}|V_{0,1}|^2}{[k_B E_M(T_S - \chi\Delta T)]^{3/2}} \frac{e^{-(\omega_0 - 2E_M)^2/4k_B E_M(T_S - \chi\Delta T)}}{1 + e^{2\omega_0/k_B(T_S - \chi\Delta T)}} \times E_M^2(1 - \chi^2)k_B\Delta T. \tag{38}$$

Equation (38) indeed implies asymmetric heat conduction provided that symmetry is broken by taking different couplings to the two baths, e.g., by taking $\chi \neq 0$. This is illustrated in Fig. 3 where the ratio $\Delta J/J_0$ is displayed against χ. It is seen that the heat conduction asymmetry can be quite

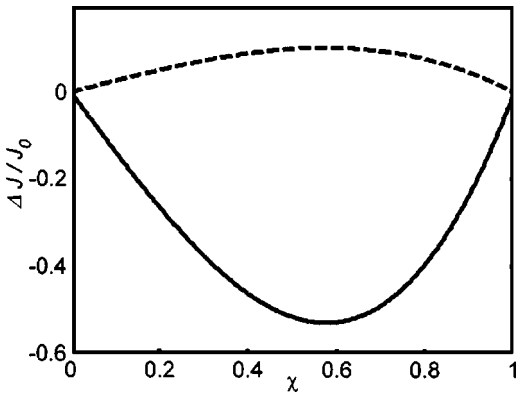

FIG. 3. Heat rectification of a TLS bridge for a nonseparable coupling, described through Eqs. (23)–(38). The ratio $\Delta J/J_0$ is plotted as a function of χ for $\omega_0=200$ cm^{-1} and $E_M=100$ cm^{-1} (dashed), and $E_M=3000$ cm^{-1} (full). The reservoir temperatures are $T_h=400$ K and $T_c=300$ K.

large, with its magnitude and sign strongly dependent on the system parameters. When $E_M \gg \omega_0$ the heat flux is dominated by the term $e^{-(\omega_0-2E_M)^2/4k_BE_M(T_S-\chi\Delta T)}$ that is bigger when ΔT is negative than when it is positive, hence the negative asymmetry in ΔJ. The same behavior is expected in the opposite, $E_M \ll \omega_0$, limit. However, when $2E_M \simeq \omega_0$ and $\omega_0 \approx k_BT_S$, J is dominated by the term $[k_BE_M(T_S-\chi\Delta T]^{-3/2}$, implying a positive asymmetry, as seen in Fig. 3.

Another interesting characteristic of this model is the strong dependence of the rectification ratio on the reorganization energy E_M, as seen in Fig. 4. Here we find that strong coupling implies strong rectification. This strong dependence on the coupling strength manifests the main difference of our model II from model I, Eqs. (2)–(21), where the ratio $\Delta J/J_0$ does not depend on the coupling strength Γ [Eq. (10)].

C. Classical Langevin dynamics

The spin-boson-type models discussed above represent examples of "very anharmonic" systems that are simple enough to yield detailed analytic solutions and thus insight about the heat rectification phenomenon. It should be emphasized that this phenomenon is the rule, not the exception, in anharmonic heat conduction. In order to demonstrate this

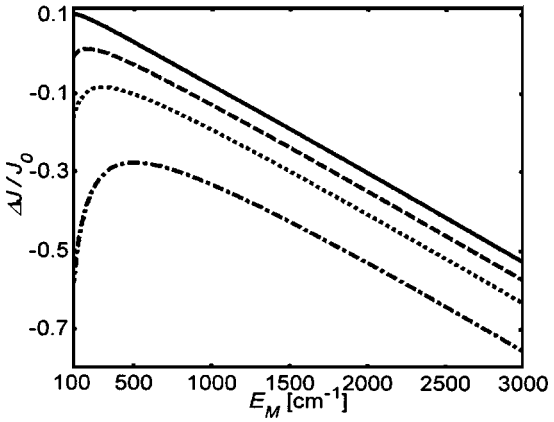

FIG. 4. The ratio $\Delta J/J_0$ plotted against E_M for $\chi=0.55$ and $\omega_0=200$ cm^{-1} (full), $\omega_0=400$ cm^{-1} (dashed), $\omega_0=600$ cm^{-1} (dotted), and $\omega_0=1000$ cm^{-1} (dot-dashed). The reservoir temperatures are $T_h=400$ K and $T_c=300$ K.

point we study next the heat conduction properties of a model system akin to a realistic molecular chain. The system includes a 1D highly anharmonic molecule composed of N identical units linking two reservoirs L and R maintained at T_L and T_R. Anharmonicity is entered by using Morse-type interactions between nearest atomic neighbors on the chain and, as before, asymmetry is included by taking different coupling strengths of the molecular chain to the L and R reservoirs.

The model Hamiltonian is given by

$$H=(2m)^{-1}\sum_{i=1}^{N} p_i^2+\sum_{i=1}^{N-1} D[e^{-\alpha(x_{i+1}-x_i-x_{eq})}-1]^2 + D[e^{-\alpha(x_1-a)}-1]^2+D[e^{-\alpha(b-x_N)}-1]^2 \tag{39}$$

supplemented by damping and noise terms operating on particle 1 and N to simulate the effect of two thermal baths. The equations of motions are

$$\ddot{x}_i=-\frac{1}{m}\frac{\partial H}{\partial x_i}, \quad i=2,3,\ldots,N-1,$$

$$\ddot{x}_1=-\frac{1}{m}\frac{\partial H}{\partial x_1}-\gamma_L\dot{x}_1+F_L(t), \tag{40}$$

$$\ddot{x}_N=-\frac{1}{m}\frac{\partial H}{\partial x_N}-\gamma_R\dot{x}_N+F_R(t).$$

In these equations a and b are constants, m is the particle mass, and the Morse parameters D, x_{eq} and α are based on the alkane C-C stretch motion as detailed below. Introducing a parameter ν to represent the level of anharmonicity in the potential, we use $D=88/\nu^2$ kcal/mole, $\alpha=1.88\nu$ Å^{-1}, $x_{eq}=1.538$ Å, and $m=m_{\text{carbon}}=12/6.02\times10^{23}$ g. In standard models for alkane force field $\nu=1$.[48] Here we artificially increase the system anharmonicity by taking $\nu>1$. The other model parameters are the friction constant γ_K $(K=L,R)$ and the bath temperatures T_L and T_R. The latter enter through the fluctuating Gaussian random forces $F_K(t)$, $K=L$, R that represent the effect of the thermal reservoirs and satisfy $\langle F_K(t)F_K(0)\rangle=2\gamma_Kk_BT_K\delta(t)/m$.

We take $\gamma_L=\gamma(1-\chi)$ and $\gamma_R=\gamma(1+\chi)$, $|\chi|\leqslant 1$, and as in Figs. 1–4, study the ratio between $\Delta J\equiv J(T_L=T_h;T_R=T_c)+J(T_L=T_c;T_R=T_h)$ and $J_0\equiv|J(\chi=0)|$ where the heat current J is calculated as the average over sites of $J_i=\langle-\dot{x}_i(\partial H_{i+1,i}/\partial x_i)\rangle$ with $H_{i+1,i}=D[e^{-\alpha(x_{i+1}-x_i-x_{eq})}-1]^2$. The average is done over steady-state trajectories computed by integrating Eq. (40) using the fourth-order Runge–Kutta method. Steady state is determined to be established when the computed heat current is the same (within numerical noise) at all sites.

The results of the calculations based on this model, displayed in Figs. 5 and 6, show that the intrinsic nonlinearity of the model is enough to induce asymmetry in the thermal conduction of the asymmetrically coupled $(\gamma_L\neq\gamma_R)$ bridge. This indicates that rectification through asymmetric chains is a general property of highly anharmonic systems. Figure 5 shows that the rectification ratio increases when the chain anharmonicity is artificially increased, while Fig. 6 presents

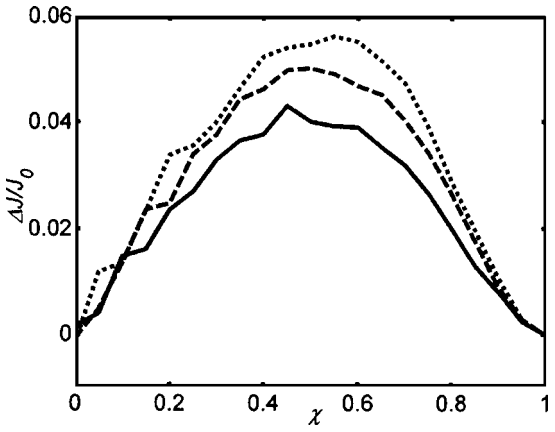

FIG. 5. The asymmetry in the thermal conduction plotted as a function of χ for a classical chain of N atoms characterized by Eqs. (39) and (40). The parameters used are $\gamma=50$ ps^{-1}, $T_h=300$ K, $T_c=0$ K, and $N=20$. The force field parameters of Eq. (39) were modified by taking v=5 (full), v=6 (dashed), and v=6.75 (dotted).

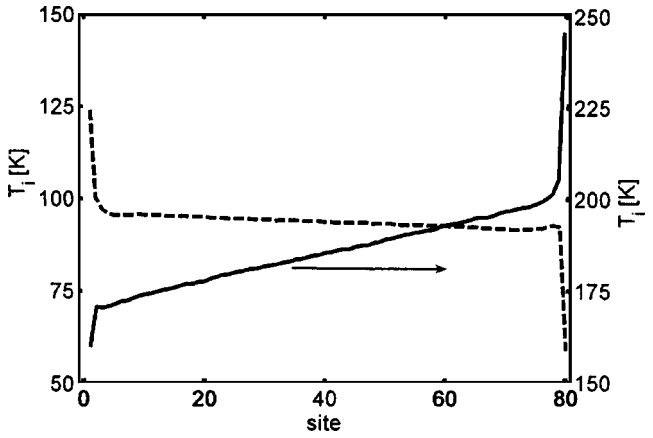

FIG. 7. The temperature profile for the $N=80$, v=6, $\gamma=50$ ps^{-1}, $\chi=0.5$ case with $T_L=T_c$; $T_R=T_h$ (full), $T_L=T_h$; $T_R=T_c$ (dashed), where $T_h=300$ K and $T_c=0$ K.

the rectification obtained for different chain sizes. The increased rectification by longest chains demonstrates that the contribution of anharmonic interactions to the thermal transport is becoming more important for longer molecules. Figure 7 demonstrates that the temperature drops essentially linearly along the chain central domain, with different slopes under the opposite temperature biases. This stands in contrast with harmonic chains where the temperature deviates from the average value, $(T_L+T_R)/2$, only at the edges.[18]

III. RECTIFICATION BY INTERNAL ASYMMETRY OF ANHARMONIC MOLECULAR MODELS

In the examples discussed above asymmetry was incorporated by taking different coupling strength between the two thermal baths and the bridging unit. Obviously, separating the overall system into these components is to some extent a matter of choice, and what appears as asymmetry in the contacts on one level of description may constitute structural asymmetry of the extended bridging unit in another. Practically, structural asymmetries in molecular bridges are easily introduced, and it is of interest to explore their effects on the heat conduction behavior of the corresponding junction. Here we describe a molecular heat rectifier based on the system anharmonicity and *internal* molecular asymmetry, which is now symmetrically coupled to the left and right thermal reservoirs. Our simplified model consists of a molecule made of two coupled nonidentical spatially separated segments N and M, each taken to be an anharmonic system and each represented by local states that are eigenstates of the isolated segment. The molecule sits as a bridge connecting two macroscopic heat reservoirs of different temperatures, see Fig. 8. We take each of the two molecular segments to couple directly to its neighboring reservoir, so that the $M(N)$ molecular residue is coupled to the left (right) reservoir of temperature $T_L(T_R)$. Direct thermal coupling between the reservoirs is assumed small and is disregarded in our following treatment. Therefore, energy can be transferred between the reservoirs only through the M-N contact.

For simplicity we assume that the temperature is low enough so that each segment can be represented by its two lowest eigenstates, i.e., each vibrational manifold is truncated to include only the two lowest-energy states, $|m_0\rangle$ and $|m_1\rangle$ of segment M and $|n_0\rangle$ and $|n_1\rangle$ of segment N, with the corresponding energies E_{m_k} and E_{n_k} $(k=0,1)$. These states are taken orthogonal, i.e., $\langle m_i|m_j\rangle=\langle n_i|n_j\rangle=\delta_{i,j}$ $(j=0,1;i=0,1)$ and complete in the sense that $\Sigma_{j=0}^{1}|m_j\rangle\langle m_j|$ and $\Sigma_{j=0}^{1}|n_j\rangle\langle n_j|$

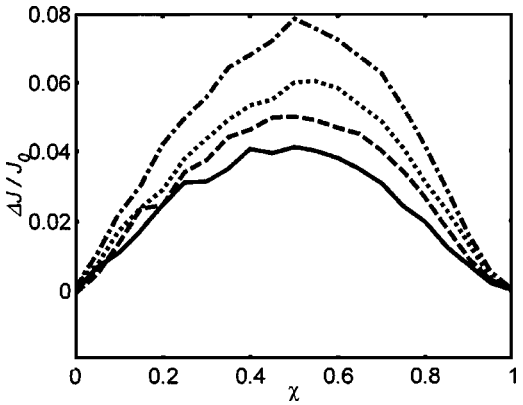

FIG. 6. Same as Fig. 5 with v=6. Full, dashed, dotted, and dot-dashed lines correspond to $N=10$, $N=20$, $N=40$, and $N=80$, respectively, with $\gamma=50$ ps^{-1}, $T_h=300$ K, and $T_c=0$ K.

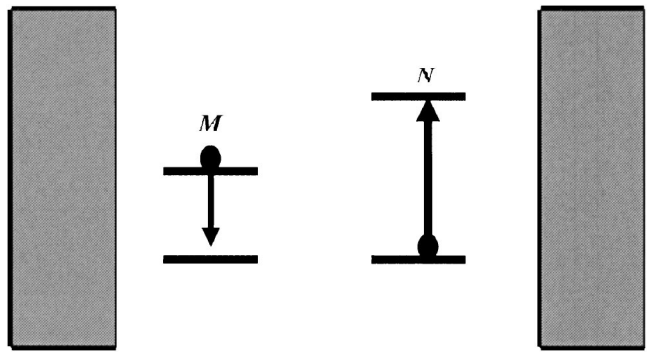

FIG. 8. A schematic representation of the model system described in Eqs. (42)–(55): two molecular species M and N whose vibrational spectrum is truncated to include only the two lowest states. The molecule is placed between two heat reservoirs of different temperatures.

are unities in their respective subspaces. Asymmetry is introduced by taking $\omega_M \neq \omega_N$: $\omega_N = E_{n_1} - E_{n_0}$; $\omega_M = E_{m_1} - E_{m_0}$ (see Fig. 8).

For definiteness take $T_L > T_R$ and assume that both temperatures are low enough so that the bridge occupies mainly its ground state. Energy transfer through the system may be viewed as a three-step process,

$$|m_0 n_0\rangle \overset{1}{\rightarrow} |m_1 n_0\rangle \overset{2}{\rightarrow} |m_0 n_1\rangle \overset{3}{\rightarrow} |m_0 n_0\rangle. \tag{41}$$

In step 1 the left heat reservoir excites the M segment to the upper vibrational state $|m_1\rangle$ while the N segment remains in its ground state. Step 2 is an $M \rightarrow N$ energy-transfer process in which M returns to its ground state while N is excited. Finally, in step 3 N returns to its ground state, transferring its energy to the right heat reservoir. A model Hamiltonian that describes this process consists of four terms,

$$H = H_S + H_B + F = H_0 + H_{M-N} + H_B + F. \tag{42}$$

The system Hamiltonian H_S includes the truncated segment Hamiltonians and the intersegment coupling,

$$H_0 = \sum_{j=0,1} E_{m_j} |m_j\rangle\langle m_j| + \sum_{j=0,1} E_{n_j} |n_j\rangle\langle n_j|, \tag{43}$$

$$H_{M-N} = V|m_0, n_1\rangle\langle m_1, n_0| + V|m_1, n_0\rangle\langle m_0, n_1|. \tag{44}$$

The Hamiltonian describing the thermal bath H_B is represented as before by a collection of harmonic oscillators $H_B = \Sigma_l \omega_l a_l^\dagger a_l + \Sigma_r \omega_r a_r^\dagger a_r$. The molecule-reservoirs coupling F is given by

$$F = F_L^\dagger |m_0\rangle\langle m_1| + F_L |m_1\rangle\langle m_0| + F_R^\dagger |n_0\rangle\langle n_1| + F_R |n_1\rangle\langle n_0|, \tag{45}$$

where $F_K (K = L, R)$ are the bath operators. A specific model for this interaction can be, for example,

$$F_K = \sum_{j \epsilon K} \frac{\alpha_j}{\sqrt{2\omega_j}} (a_j^\dagger + a_j), \quad K = L, R. \tag{46}$$

The coefficients $\alpha_j (j = l, r)$ are the molecule-reservoir coupling strengths. While in Sec. II asymmetry was incorporated by taking $\alpha_j (j \epsilon L) \neq \alpha_j (j \epsilon R)$, here they are taken to be the same. With this form of the coupling, Eqs. (45) and (46), the present model is closely related to the first spin-boson configuration of Sec. II, see Eqs. (4) and (5). Indeed we show below that these two heat transport models are related.

We proceed by defining the four states ($|a\rangle = |m_0, n_0\rangle, |b\rangle = |m_0, n_1\rangle, |c\rangle = |m_1, n_0\rangle, |d\rangle = |m_1, n_1\rangle$). These are eigenstates of a system comprising the two uncoupled molecular segments with energies $E_a = E_{m_0} + E_{n_0}$; $E_b = E_{m_0} + E_{n_1}$; $E_c = E_{m_1} + E_{n_0}$; $E_d = E_{m_1} + E_{n_1}$. In states $|a\rangle$ and $|d\rangle$ both TLS are in their ground or excited vibrational states, respectively, whereas $|b\rangle$ and $|c\rangle$ represent states in which one segment is excited while the other is in its ground state. The different components of the Hamiltonian (42) in this representation are

$$H_0 = E_a |a\rangle\langle a| + E_b |b\rangle\langle b| + E_c |c\rangle\langle c| + E_d |d\rangle\langle d|, \tag{47}$$

$$H_{M-N} = V|b\rangle\langle c| + V|c\rangle\langle b|, \tag{48}$$

$$H_B = \sum_l \omega_l a_l^\dagger a_l + \sum_r \omega_r a_r^\dagger a_r, \tag{49}$$

$$F = F_L^\dagger [|a\rangle\langle c| + |b\rangle\langle d|] + F_L [|c\rangle\langle a| + |d\rangle\langle b|] + F_R^\dagger [|a\rangle\langle b| + |c\rangle\langle d|] + F_R [|b\rangle\langle a| + |d\rangle\langle c|]. \tag{50}$$

Let C be the matrix that diagonalizes the molecular Hamiltonian $H_S = H_0 + H_{M-N}$, i.e.,

$$H_S = C^{-1} D C, \tag{51}$$

where D is the diagonal eigenenergy matrix. The matrix C transforms between the diagonal basis ($|a\rangle|i\rangle|j\rangle|d\rangle$) and the local basis ($|a\rangle|b\rangle|c\rangle|d\rangle$). For the details see the Appendix. In the new basis the molecular states are uncoupled and transitions between them can be caused only by their mutual interactions with the thermal baths.

Next we calculate the heat current flowing through the system. We focus on the regime of incoherent transport, assuming that dephasing is fast so that the dynamics can be described by rate equations (master equation) for the populations $P_s, s = (a, i, j, d)$ of the diagonalized states. This master equation takes the form

$$\begin{aligned}
\dot{P}_a &= (k_{i\to a}^L + k_{i\to a}^R) P_i + (k_{j\to a}^L + k_{j\to a}^R) P_j - (k_{a\to i}^L + k_{a\to i}^R \\
&\quad + k_{a\to j}^L + k_{a\to j}^R) P_a, \\
\dot{P}_i &= (k_{a\to i}^L + k_{a\to i}^R) P_a + (k_{d\to i}^L + k_{d\to i}^R) P_d - (k_{i\to a}^L + k_{i\to a}^R \\
&\quad + k_{i\to d}^L + k_{i\to d}^R) P_i, \\
\dot{P}_j &= (k_{a\to j}^L + k_{a\to j}^R) P_a + (k_{d\to j}^L + k_{d\to j}^R) P_d - (k_{j\to a}^L + k_{j\to a}^R \\
&\quad + k_{j\to d}^L + k_{j\to d}^R) P_j, \\
\dot{P}_d &= (k_{i\to d}^L + k_{i\to d}^R) P_i + (k_{j\to d}^L + k_{j\to d}^R) P_j - (k_{d\to i}^L + k_{d\to i}^R \\
&\quad + k_{d\to j}^L + k_{d\to j}^R) P_d,
\end{aligned} \tag{52}$$

where the explicit expressions for the rates constants are given in the Appendix. For example, the rate coefficient $k_{a\to i}^L$ for the $|a\rangle \rightarrow |i\rangle$ excitation process driven by the left heat reservoirs is

$$k_{a\to i}^L = 2\pi |C_{2,3}|^2 \rho_L (E_{i,a}) n_L (E_{i,a}) \left. \frac{\alpha_l^2}{2\omega_l} \right|_{E_{i,a}}. \tag{53}$$

It is expressed in terms of the matrix elements of C, defined in Eq. (51), the L reservoir density of modes $\rho_L(E)$, the thermal occupation of the bath states $n_L(E)$, and the system-bath coupling strength α_l, all calculated at the energy difference $E_{i,a} \equiv E_i - E_a$.

The steady-state solution of Eq. (52) is obtained by taking the time derivatives in Eq. (52) to zero and applying the probability conservation condition $P_{m_0} + P_{m_1} = 1$; $P_{n_0} + P_{n_1} = 1$ that implies that each segment must occupy either the lower or the upper state. In the diagonalized basis this condition is translated into $P_a + P_i + P_j + P_d = 1$. The heat current is defined in the incoherent regime as the net heat exchange

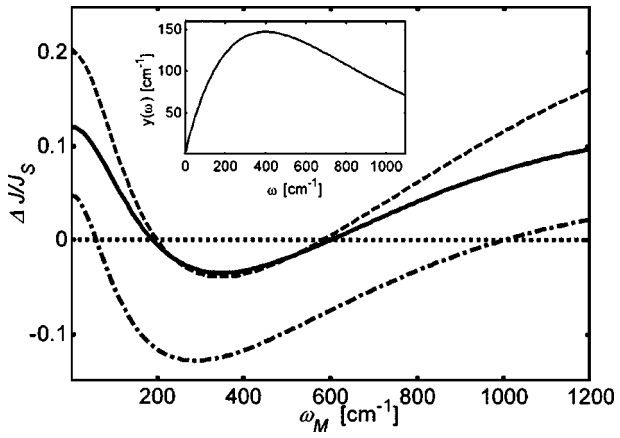

FIG. 9. The ratio $\Delta J/J_s$ plotted against the frequency ω_M for different frequencies of the N component: $\omega_N=200$ cm^{-1} (dashed), $\omega_N=600$ cm^{-1} (full), and $\omega_N=1000$ cm^{-1} (dot-dashed). $T_h=500$ K, $T_c=300$ K, and $\omega_c=400$ cm^{-1}. Inset: the function $y(\omega)=\omega e^{-\omega/\omega_c}$ vs ω for cutoff frequency $\omega_c=400$ cm^{-1}.

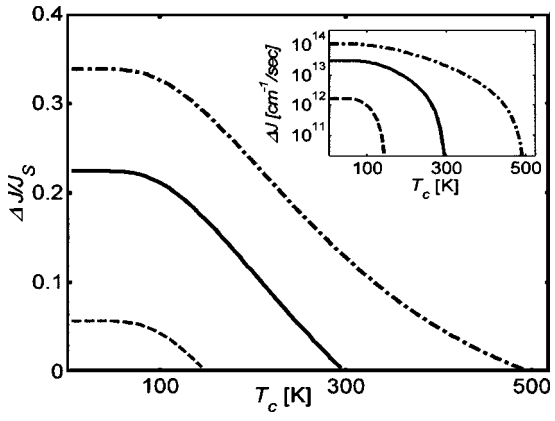

FIG. 10. Rectification ratio as a function of T_c. The hot bath is maintained at $T_h=150$ K (dashed); $T_h=300$ K (full); $T_h=500$ K (dot-dashed). Other parameters are $\omega_M=1000$ cm^{-1}, $\omega_N=300$ cm^{-1}, and $\omega_c=400$ cm^{-1}. Inset: the sum of the (oppositely going) heat currents for the corresponding cases.

between the molecular segments and the reservoirs. It is given by multiplying the microscopic rate of population transfer by the energy transferred. In the following expression the heat current is calculated at the left contact and a sign notation is adopted by which positive (negative) terms represent excitation (relaxation) processes on the molecule,

$$J=[(k^L_{a\to i}E_{i,a}+k^L_{a\to j}E_{j,a})P_a+k^L_{i\to d}E_{d,i}P_i+k^L_{j\to d}E_{d,j}P_j] - [k^L_{i\to a}E_{i,a}P_i+k^L_{j\to a}E_{j,a}P_j+(k^L_{d\to i}E_{d,i}+k^L_{d\to j}E_{d,j})P_d]. \tag{54}$$

Consequently, a positive J is associated with the heat flux from left to right. An equivalent expression for J can be written at the right contact,

$$J=-[(k^R_{a\to i}E_{i,a}+k^R_{a\to j}E_{j,a})P_a+k^R_{i\to d}E_{d,i}P_i+k^R_{j\to d}E_{d,j}P_j] + [k^R_{i\to a}E_{i,a}P_i+k^R_{j\to a}E_{j,a}P_j+(k^R_{d\to i}E_{d,i}+k^R_{d\to j}E_{d,j})P_d]. \tag{55}$$

At steady state Eqs. (54) and (55) yield identical results.

The rectifying behavior of the model is next analyzed in terms of the ratio $f\equiv\Delta J/J_s$ where $\Delta J\equiv J(T_L=T_h;T_R=T_c)+J(T_L=T_c;T_R=T_h)$ and $J_s\equiv|J(T_L=T_h;T_R=T_c)|+|J(T_L=T_c;T_R=T_h)|$ and where T_h and T_c denote the high and low temperatures that characterize the thermally biased junction. In the limit $f=0$ there is no rectification, while $|f|=1$ implies full rectification, where heat can be transferred only in one direction. Figures 9 and 10 present our results. The typical parameters used are ω_M, $\omega_N\approx 100$–1000 cm^{-1} and coupling V in the range of 10–50 cm^{-1}. In the calculation of thermal rates, such as Eq. (53) (see the Appendix), we employ the Debye model for the reservoir density of modes,

$$\rho_K(\omega)=N_B\frac{\omega^2}{2\omega_c^3}e^{-\omega/\omega_c},\quad K=L,R. \tag{56}$$

Here N_B is the number of the reservoir modes and ω_c is the Debye cutoff frequency, taken to be identical for the two reservoirs L and R. Within this model the rate coefficient (53) becomes

$$k^L_{s'\to s}\propto\left.\frac{\pi\alpha_l^2}{\omega_l}\right|_\omega n_L(\omega)\rho_L(\omega)=\kappa\omega e^{-\omega/\omega_c}n_L(\omega), \tag{57}$$

where $\omega=E_s-E_s$, and $\kappa\equiv N_B(\pi\alpha_l^2/2\omega_c^3)_\omega$ is assumed to be equal for the two reservoirs and for all modes. In the calculations depicted in Figs. 9 and 10 we have taken $\kappa=1$ and have used the cutoff frequencies in the range of $\omega_c=200$–800 cm^{-1}. With these parameters the resulting rate constants are about $(50$–$300)n_L(\omega)$ cm^{-1} for ω in the 100-1200-cm^{-1} range.

Figure 9 shows the rectification ratio $f=\Delta J/J_S$ as a function of the level spacing ω_M of the left TLS segment for different ω_N values: 200, 600, and 1000 cm^{-1}. The parameters $V=50$ cm^{-1}, $T_c=300$ K, $T_h=500$ K, and $\omega_c=400$ cm^{-1} are used in this calculation. The line $f=0$ is also plotted to enable easy identification of points of no rectification. We find that the ratio f changes its sign from positive to negative and again to positive as the frequency ω_M is varied. Note that positive f means that in absolute values, the current is larger when $T_L>T_R$ than in the opposite case.

In spite of this apparently complicated dependence on ω_M, this behavior of the rectification ratio f is in accordance with the results of the first spin-boson model presented in Sec. II. There we found that the heat current is larger when the bridge links more strongly to the colder reservoir than when it is coupled more strongly to the hotter one. This observation holds also here, however, in the present case, the effective molecule-bath couplings, as expressed by the associated rate coefficients, e.g., Eq. (57), have a complicated structure. As a simplification we note that for the range of temperatures and frequencies used, the thermal factor n_K is of the order of one. The system-bath interaction can therefore be fully absorbed in the frequency-dependent function $y(\omega)=\omega e^{-\omega/\omega_c}$ so that $k^L_{s'\to s}\propto y(\omega)$, see Eq. (57). This function is plotted in the inset of Fig. 9 for $\omega_c=400$ cm^{-1}. Below its maximum at $\omega=\omega_c$ the function $y(\omega)$ gets the same value at two different frequencies. For example, $y(\omega=200)=y(\omega=700)$. We expect therefore that for these two frequencies the effective system-bath coupling should be similar. This information enables us to interpret the behavior of f in Fig. 9: while the frequency of the right TLS segment is held fixed,

i.e., the effective interaction to the right reservoir is constant, the frequency of the left TLS segment is varied, modifying effectively the coupling strength to the L bath. Thus, for $\omega_N=200\ \mathrm{cm}^{-1}$, the effective coupling to the L bath is smaller than that to the R bath if $\omega_M<200\ \mathrm{cm}^{-1}$, larger than it for $200<\omega_M<700$ and again smaller for $\omega_M>700\ \mathrm{cm}^{-1}$. For these ranges we expect therefore (similarly to the separable single TLS model) to obtain positive rectification ratio, negative and again positive values, respectively. Indeed we find in Fig. 9 (dashed line) the following ranges of behavior:

$$\begin{aligned} &f>0 \quad \text{for } 0<\omega_M<200,\\ &f<0 \quad \text{for } 200<\omega_M<580,\\ &f>0 \quad \text{for } \omega_M>580. \end{aligned} \tag{58}$$

The same rule is obeyed for $\omega_N=600\ \mathrm{cm}^{-1}$ (full line), where here as $y(600)\sim y(250)$, we expect to get zero rectification also for $\omega_M=250\ \mathrm{cm}^{-1}$. For $250\ \mathrm{cm}^{-1}<\omega_M<600\ \mathrm{cm}^{-1}$, the effective coupling between the left bath and its neighboring TLS segment is stronger than the corresponding coupling on the right and f should be negative, as indeed observed in Fig. 9. Similar arguments can explain the dashed-dotted $\omega_N=1000\ \mathrm{cm}^{-1}$ curve. Smaller values of the coherent coupling V and larger cutoff frequencies lead basically to the same behavior.

It should be emphasized that the above argument is only qualitative. First, the frequency dependence of the occupation factors in the rate constant cannot really be ignored, particularly not in the low- or very high-temperature regimes. Also, the actual calculation is done in the diagonalized representations where the states are coupled to both hot and cold reservoirs, and arguments based on the local state representation picture can provide only qualitative, though intuitively appealing, understanding.

Finally, Fig. 10 presents the temperature dependence of rectification. We get the results similar to those observed in Fig. 1 for the separable TLS with the asymmetrical coupling. The inset shows for reference the absolute value of ΔJ.

To conclude this section we emphasize three observations: (i) asymmetry in the present model was incorporated via inherent molecular asymmetry that indirectly controls the effective molecule-bath coupling. (ii) Even in the presence of such structural asymmetry rectification will not be observed when the effective system-bath couplings at the right and left contacts are the same. (iii) Large rectification ratios appear for $\omega_M \gg \omega_N$ or $\omega_N \gg \omega_M$. However, for such cases the absolute current J may be small.

IV. CONCLUSIONS

While most theoretical investigations on nanowire transport focus on electronic conduction properties, thermal transport characteristics of these devices are also of interest for various applications. We have focused here on molecular level heat rectifiers, showing partial inhibition of heat flow in one direction of the temperature bias, due to asymmetric nonlinear interactions. This effect cannot exist in harmonic chains, even in the presence of structural asymmetry. Taking into account anharmonic interactions, we have described several types of heat rectifiers, where asymmetry was imposed either through different coupling to the contacts or by internal molecular asymmetry. In the first model anharmonicity results from the character of a two-level system and asymmetry stems from different interaction strengths with the thermal baths. Two variants of this spin-boson model were considered: separable, where the reservoirs interact additively with the bridge, and nonseparable. For both cases approximate analytical solutions for the heat current/temperature-bias characteristics of the junction were obtained. We have also demonstrated numerically, using Langevin dynamics simulations, that an anharmonic molecular chain coupled asymmetrically to the thermal baths, rectifies heat, and that this effect is stronger for longer chains. Asymmetrical coupling to the two thermal reservoirs can be implemented by using different thermal contacts, either through different coupling strengths or through the differences in the Debye temperatures of these contacts. The latter affects the matching between the vibrational spectra of the bridge and the reservoirs. Finally, we have considered a model where asymmetry is related to the internal level structure of the molecule. In the example studied this asymmetry reflects the asymmetrical spatial organization of molecular nuclear motions. We have explained the nontrivial rectification behavior of this model in terms of an effective system-bath coupling.

In conclusion, we have found that heat rectification is a basic property of any realistic asymmetric junction, since vibrational anharmonicity is always presented at some degree. Clearly, for a practical device, this kind of behavior should be optimized by controlling the structural parameters.[49]

ACKNOWLEDGMENTS

This research was supported by the Israel National Science Foundation, by the U.S.—Israel Binational Science Foundation and by the Wolkswagen Foundation.

APPENDIX: DERIVATION OF THE MASTER EQUATION [EQ. (52)] AND THE RATE CONSTANTS

We derive here the master equation Eq. (52) from the model Hamiltonian Eqs. (47)–(50) and give the explicit expressions for the rate constants. We start by diagonalizing the molecular Hamiltonian H_S, defined in Eqs. (47) and (48), given in terms of the states $|a\rangle,|b\rangle,|c\rangle,|d\rangle$. Note that only the states $|b\rangle$ and $|c\rangle$ are coupled to each other, while the states $|a\rangle$ and $|d\rangle$ are already eigenstates of the system Hamiltonian. Diagonalization $H_S=C^{-1}DC$ leads to the new four eigenvectors denoted by $|a\rangle,|i\rangle,|j\rangle,|d\rangle$, related to the old basis through

$$\begin{aligned} |a\rangle &= |a\rangle,\\ |b\rangle &= C_{2,2}|i\rangle + C_{2,3}|j\rangle,\\ |c\rangle &= C_{3,2}|i\rangle + C_{3,3}|j\rangle,\\ |d\rangle &= |d\rangle, \end{aligned} \tag{A1}$$

where C_{ij} are the ij elements of the transformation matrix C. The elements of the diagonal matrix D are the relevant molecular energy levels, E_a, E_i, E_j, and E_d. The system-bath interaction term, Eq. (50), is next written in terms of the diagonalized basis,

$$F_L^\dagger[|a\rangle\langle c| + |b\rangle\langle d|] = F_L^\dagger[C_{3,2}^*|a\rangle\langle i| + C_{3,3}^*|a\rangle\langle j| + C_{2,2}|i\rangle\langle d| + C_{2,3}|j\rangle\langle d|],$$

$$F_L[|c\rangle\langle a| + |d\rangle\langle b|] = F_L[C_{3,2}|i\rangle\langle a| + C_{3,3}|j\rangle\langle a| + C_{2,2}^*|d\rangle\langle i| + C_{2,3}^*|d\rangle\langle j|], \tag{A2}$$

$$F_R^\dagger[|a\rangle\langle b| + |c\rangle\langle d|] = F_R^\dagger[C_{2,2}^*|a\rangle\langle i| + C_{2,3}^*|a\rangle\langle j| + C_{3,2}|i\rangle\langle d| + C_{3,3}|j\rangle\langle d|],$$

$$F_R[|b\rangle\langle a| + |d\rangle\langle c|] = F_R[C_{2,2}|i\rangle\langle a| + C_{2,3}|j\rangle\langle a| + C_{3,2}^*|d\rangle\langle i| + C_{3,3}^*|d\rangle\langle j|].$$

The complete Hamiltonian in its diagonalized form is

$$H = H_B + \tilde{H}_S + F, \tag{A3}$$

where the bath term H_B is given in Eq. (49). The system Hamiltonian is

$$\tilde{H}_S = E_a|a\rangle\langle a| + E_i|i\rangle\langle i| + E_j|j\rangle\langle j| + E_d|d\rangle\langle d|. \tag{A4}$$

The molecule-reservoir coupling terms are given in (A2). The master equations describing the dynamics of the molecular states are written next. We assume that the dynamics is well described by the states population and that coherent effects can be neglected. Systematic derivation of the system equations of motion is done by applying the Redfield approximation,[40] neglecting the nondiagonal terms of the density matrix, assuming their fast decay. This leads to the rate equations,

$$\dot{P}_a = (k_{i\to a}^L + k_{i\to a}^R)P_i + (k_{j\to a}^L + k_{j\to a}^R)P_j - (k_{a\to i}^L + k_{a\to i}^R + k_{a\to j}^L + k_{a\to j}^R)P_a,$$

$$\dot{P}_i = (k_{a\to i}^L + k_{a\to i}^R)P_a + (k_{d\to i}^L + k_{d\to i}^R)P_d - (k_{i\to a}^L + k_{i\to a}^R + k_{i\to d}^L + k_{i\to d}^R)P_i, \tag{A5}$$

$$\dot{P}_j = (k_{a\to j}^L + k_{a\to j}^R)P_a + (k_{d\to j}^L + k_{d\to j}^R)P_d - (k_{j\to a}^L + k_{j\to a}^R + k_{j\to d}^L + k_{j\to d}^R)P_j,$$

$$\dot{P}_d = (k_{i\to d}^L + k_{i\to d}^R)P_i + (k_{j\to d}^L + k_{j\to d}^R)P_j - (k_{d\to i}^L + k_{d\to i}^R + k_{d\to j}^L + k_{d\to j}^R)P_d,$$

where P_k, $(k=a,i,j,d)$ are the state populations. The rate coefficients are given as Fourier transform of the bath correlation functions. For example,

$$k_{j\to a}^L = |C_{3,3}|^2 \int_{-\infty}^{\infty} e^{-iE_{j,a}t}\langle F_L(0)F_L^\dagger(t)\rangle dt. \tag{A6}$$

In the linear coupling model, using Eq. (46), this leads to

$$\begin{aligned} k_{j\to a}^L &= |C_{3,3}|^2 \int_{-\infty}^{\infty} e^{-iE_{j,a}t} \sum_l \frac{a_l^2}{2\omega_l} \\ &\quad \times \{n_L(\omega_l)e^{-i\omega_l t} + [n_L(\omega_l)+1]e^{i\omega_l t}\}dt \\ &= |C_{3,3}|^2 \sum_l \frac{\pi a_l^2}{\omega_l}\{n_L(-E_{j,a})\delta(E_{j,a}+\omega_l) \\ &\quad + [n_L(E_{j,a})+1]\delta(E_{j,a}-\omega_l)\} \end{aligned} \tag{A7}$$

and an analogous expression at the right side,

$$\begin{aligned} k_{j\to a}^R &= |C_{2,3}|^2 \int_{-\infty}^{\infty} e^{-iE_{j,a}t}\langle F_R(0)F_R^\dagger(t)\rangle dt \\ &= |C_{2,3}|^2 \sum_r \frac{\pi \alpha_r^2}{\omega_r}\{n_R(-E_{j,a})\delta(E_{j,a}+\omega_r) + [n_R(E_{j,a}) \\ &\quad + 1]\delta(E_{j,a}-\omega_r)\}. \end{aligned} \tag{A8}$$

Note that though in principle we have to trace over both reservoir degrees of freedom, in practice in the linear coupling model we trace always only on one of the thermal baths: in Eq. (A7) over the L reservoir and in (A8) over the R side. There are no mixed contributions such as $\langle F_L F_R\rangle$ since these terms are zero for the system-bath interaction model (45) and (46). In the limit where the coupling V is small compared to the vibrational frequencies, the following inequalities hold:

$$E_j > E_a, \quad E_i > E_a. \tag{A9}$$

Antirotating wave terms are therefore neglected and the rate constant (A7) is written as

$$k_{j\to a}^L = |C_{3,3}|^2[n_L(E_{j,a})+1]\rho_L(E_{j,a}) \left.\frac{\pi\alpha_l^2}{\omega_l}\right|_{\omega_l=E_{j,a}}, \tag{A10}$$

where ρ_L is the density of states of the L reservoir. The rest of the rate constants in the master equations (A5) are calculated in an analogous way. They depend on the diagonalization elements C, the molecule-reservoir coupling parameters α_l and α_r, the reservoir density of vibrational states $\rho_K(E)$, $K=L$, R, and the bath thermal distribution. Denoting

$$\lambda_L(E) \equiv \left.\frac{\alpha_l^2}{2\omega_l}\right|_E, \quad \lambda_R(E) \equiv \left.\frac{\alpha_r^2}{2\omega_r}\right|_E. \tag{A11}$$

The rate constants in (A5) then take the form

$$\begin{aligned}
k^K_{a\to i} &= 2\pi\lambda_K(E_{i,a})\rho_K(E_{i,a})n_K(E_{i,a})[|C_{2,3}|^2\delta_{L,K} \\
&\quad + |C_{2,2}|^2\delta_{R,K}], \\
k^K_{a\to j} &= 2\pi\lambda_K(E_{j,a})\rho_K(E_{j,a})n_K(E_{j,a})[|C_{3,3}|^2\delta_{L,K} \\
&\quad + |C_{2,3}|^2\delta_{R,K}], \\
k^K_{i\to d} &= 2\pi\lambda_K(E_{d,i})\rho_K(E_{d,i})n_K(E_{d,i})[|C_{2,2}|^2\delta_{L,K} \\
&\quad + |C_{2,3}|^2\delta_{R,K}], \\
k^K_{j\to d} &= 2\pi\lambda_K(E_{d,j})\rho_K(E_{d,j})n_K(E_{d,j})[|C_{2,3}|^2\delta_{L,K} \\
&\quad + |C_{3,3}|^2\delta_{R,K}],
\end{aligned} \tag{A12}$$

and

$$k^K_{p\to q} = k^K_{q\to p}e^{\beta_K E_{p,q}}, \quad p,q = a,d,i,j, \quad K = L,R. \tag{A13}$$

[1] A. Aviram and M. A. Ratner, Chem. Phys. Lett. **29**, 277 (1974).
[2] C. Zhou, M. R. Deshpande, M. A. Reed, L. Jones-II, and J. M. Tour, Appl. Phys. Lett. **71**, 611 (1997).
[3] R. M. Metzger, J. Mater. Chem. **9**, 2027 (1999); **10**, 55 (2000).
[4] C. Krzeminski, C. Delerue, G. Allan, D. Vuillaume, and R. M. Metzger, Phys. Rev. B **64**, 085405 (2001).
[5] S. T. Yau, C. Zhang, and P. C. Innis, J. Chem. Phys. **112**, 6774 (2000).
[6] E. Geva and R. Kosloff, J. Chem. Phys. **96**, 3054 (1992); **97**, 4398 (1992); **104**, 7681 (1996).
[7] T. Feldmann and R. Kosloff, Phys. Rev. E **65**, 055102 (2002); **68**, 016101 (2003).
[8] M. O. Scully, Phys. Rev. Lett. **87**, 220601-1 (2001).
[9] F. Jülicher, A. Ajdari, and J. Prost, Rev. Mod. Phys. **69**, 1269 (1997).
[10] V. Balzani, M. Gómez-López, and J. F. Stoddart, Acc. Chem. Res. **31**, 405 (1998).
[11] I. Bargatin and M. L. Roukes, Phys. Rev. Lett. **91**, 138302 (2003).
[12] D. G. Cahill, K. Goodson, and A. Majumdar, J. Heat Transfer **124**, 223 (2002).
[13] L. Shi and A. Majumdar, J. Heat Transfer **124**, 329 (2002).
[14] P. Kim, L. Shi, A. Majumdar, and P. L. McEuen, Phys. Rev. Lett. **87**, 215502 (2001).
[15] D. J. Nesbitt and R. W. Field, J. Phys. Chem. **100**, 12735 (1996).
[16] D. Schwarzer, C. Hanisch, P. Kutne, and J. Troe, J. Phys. Chem. A **106**, 8019 (2002).
[17] D. Schwarzer, P. Kutne, C. Schröder, and J. Troe, J. Chem. Phys. **121**, 1754 (2004).
[18] Z. Rieder, J. L. Lebowitz, and E. Lieb, J. Math. Phys. **8**, 1073 (1967).
[19] U. Zürcher and P. Talkner, Phys. Rev. A **42**, 3278 (1990).
[20] A. Casher and J. L. Lebowitz, J. Math. Phys. **12**, 1701 (1971).
[21] A. J. O'Connor and J. L. Lebowitz, J. Math. Phys. **15**, 692 (1974).
[22] D. M. Leitner and P. G. Wolynes, Phys. Rev. E **61**, 2902 (2000).
[23] S. Lepri, R. Livi, and A. Politi, Phys. Rev. Lett. **78**, 1896 (1997).
[24] F. Mokross and H. Buttner, J. Phys. C **16**, 4539 (1983).
[25] B. Hu, B. Li, and H. Zhao, Phys. Rev. E **57**, 2992 (1998).
[26] S. Lepri, R. Livi, and A. Politi, Phys. Rep. **377**, 1 (2003).
[27] L. G. C. Rego and G. Kirczenow, Phys. Rev. Lett. **81**, 232 (1998).
[28] K. Schwab, E. A. Henriksen, J. M. Worlock, and M. L. Roukes, Nature (London) **404**, 974 (2000).
[29] A. Ozpineci and S. Ciraci, Phys. Rev. B **63**, 125415 (2001).
[30] D. Segal, A. Nitzan, and P. Hänggi, J. Chem. Phys. **119**, 6840 (2003).
[31] Q. F. Sun, P. Yang, and H. Guo, Phys. Rev. Lett. **89**, 175901 (2002).
[32] R. Landauer, IBM J. Res. Dev. **1**, 223 (1957).
[33] W. Tian, S. Datta, S. Hong, R. Reifenberger, J. I. Henderson, and C. P. Kubiak, J. Chem. Phys. **109**, 2874 (1998).
[34] V. Mujica, M. A. Ratner, and A. Nitzan, Chem. Phys. **281**, 147 (2002).
[35] M. Terraneo, M. Peyrard, and G. Casati, Phys. Rev. Lett. **88**, 094302 (2002).
[36] D. Segal and A. Nitzan, Phys. Rev. Lett. **94**, 034301 (2005).
[37] J. Taylor, M. Brandbyge, and K. Stokbro, Phys. Rev. Lett. **89**, 138301 (2002).
[38] D. M. Leitner, Phys. Rev. Lett. **87**, 188102 (2001).
[39] H. Grabert and A. Nitzan, Chem. Phys. **296**, 101 (2004).
[40] A. G. Redfield, IBM J. Res. Dev. **1**, 19 (1957).
[41] Equation (6) is derived assuming $\langle B\rangle = 0$, which is exact in the linear coupling limit, Eq. (5). In the strong coupling case discussed below, $\langle B\rangle \neq 0$ leads to an additional coherent transfer route which is, however, strongly damped and may be disregarded; see, e.g., D. Segal and A. Nitzan, Chem. Phys. **281**, 235 (2002).
[42] Note that the result Eq. (15) holds only for small $\Gamma_K (K = L, R)$ because the broadening of the oscillator frequency was not taken into account. The result of the full quantum treatment of Ref. 30 $\mathcal{T}(\omega) = (2/\pi)\omega^2\Gamma_L\Gamma_R[(\omega^2 - \omega_0^2)^2 + (\Gamma_L + \Gamma_R)^2\omega^2]^{-1}$ remains finite in the limit $\Gamma_K \to \infty$. For the analogous consideration in the electron conduction case see Ref. 44.
[43] N. S. Wingreen, K. W. Jacobsen, and J. W. Wilkins, Phys. Rev. B **40**, 11834 (1989).
[44] S. Datta, Nanotechnology **15**, S433 (2004).
[45] G. D. Mahan, *Many-Particle Physics* (Plenum, New York, 2000).
[46] R. A. Marcus, J. Chem. Phys. **24**, 966 (1956).
[47] It can be easily verified that the same result is obtained from the expression for the heat flux out of the left bath.
[48] S. Lifson and P. S. Stem, J. Chem. Phys. **77**, 4542 (1982).
[49] B. Li, L. Wang, and G. Casati, Phys. Rev. Lett. **93**, 184301 (2004).